Binding of Aβ peptide creates lipid density depression in DMPC bilayer

CrossMark

Christopher Lockhart, Dmitri K. Klimov *

School of Systems Biology, George Mason University, Manassas, VA 20110, United States

ABSTRACT

Using isobaric–isothermal replica exchange molecular dynamics and all-atom explicit water model we study the impact of Aβ monomer binding on the equilibrium properties of DMPC bilayer. We found that partial insertion of Aβ peptide into the bilayer reduces the density of lipids in the binding "footprint" and indents the bilayer thus creating a lipid density depression. Our simulations also reveal thinning of the bilayer and a decrease in the area per lipid in the proximity of Aβ. Although structural analysis of lipid hydrophobic core detects disordering in the orientations of lipid tails, it also shows surprisingly minor structural perturbations in the tail conformations. Finally, partial insertion of Aβ monomer does not enhance water permeation through the DMPC bilayer and even causes considerable dehydration of the lipid–water interface. Therefore, we conclude that Aβ monomer bound to the DMPC bilayer fails to perturb the bilayer structure in both leaflets. Limited scope of structural perturbations in the DMPC bilayer caused by Aβ monomer may constitute the molecular basis of its low cytotoxicity.

© 2014 Elsevier B.V. All rights reserved.

1. Introduction

The onset of Alzheimer's disease (AD) is linked to Aβ peptides, which are the products of normal cellular proteolysis [1]. Depending on the specific location where Aβ is cleaved from the amyloid precursor protein, two main Aβ alloforms, Aβ1-40 and Aβ1-42, are identified, of which the former represents about 90% of all Aβ species in cerebrospinal fluid [2]. Experimental data demonstrate that Aβ peptides, particularly in oligomeric forms, exert cytotoxic effects on neuron cells [3,4]. Yet, from the molecular perspective it is still unclear how Aβ peptides induce damage to cells causing their death. It is reasonable to suggest that Aβ oligomers may disrupt cellular membranes and increase their permeability to ions, particularly Ca^{2+} [5]. Along these lines of thought, theoretical models propose that Aβ aggregates inside the lipid bilayers form stable pores, which lead to uncontrollable ion traffic [6,7]. Independent of specific mode of membrane perturbation, the interactions of Aβ peptides with membranes are likely to destabilize cellular ion homeostasis.

Numerous experimental studies have probed Aβ interactions with lipid bilayers [8–15]. It appears that at low Aβ concentrations (≲150 nM) Aβ peptides bind to lipid bilayers as monomers [13], but at higher peptide concentrations Aβ oligomeric species interact with the bilayers [12]. Furthermore, Aβ oligomers display strongest binding affinity compared to large aggregates [16] and Aβ binding affinity to anionic lipid bilayers is larger than for zwitterionic ones [17]. Aβ peptides not only bind but also penetrate into the core of

lipid bilayers. This conclusion follows from the analysis of electron density profiles, which indicates that Aβ1-40 interacts with bilayer hydrophobic cores [9]. Binding of Aβ peptides to the lipid bilayers and penetration into their cores compromise the integrity of bilayers. In the extreme case Aβ peptides can completely destabilize DMPC bilayers transforming lamellar phase into micelles [18]. However, more typically the impact of Aβ peptides is limited to perturbation of bilayer structure and increased permeability of ions [14]. Importantly, deep penetration of Aβ into the bilayer causes more profound disruption of its structure compared to surface binding [8,15]. In support of theoretical models, application of atomic force microscopy and circular dichroism suggests that Aβ peptides can form stable structures resembling ion channels in the bilayers [12].

All-atom explicit water molecular dynamics (MD) is a useful, complementary to experiments, tool offering unparalleled opportunities to probe Aβ-bilayer interactions in atomic detail. Constant temperature MD simulations have investigated the lipid bilayers with preinserted Aβ peptides and performed the analysis of Aβ impact on the bilayer structure [19–21]. These studies have showed that Aβ peptides, even in monomeric form, significantly disorder lipid structure and packing. Although Aβ monomers generally remained embedded in the zwitterionic DPPC or POPC lipid bilayers for the duration of simulations (several hundreds of ns), they also revealed a tendency to move closer to the bilayer surface [19]. One published report has even observed expulsion of Aβ peptide from the lipid bilayer and its readsorption on the surface [22]. Recent MD study utilizing umbrella sampling has revealed that Aβ peptides bound to the bilayer stabilize the formation of pores [23]. Furthermore, MD simulations have probed Aβ aggregation in the lipid bilayers showing that Aβ monomers can form mobile small oligomers,

* Corresponding author. Tel.:+1 703 993 8395; fax: +1 703 993 8401.
E-mail address: dklimov@gmu.edu (D.K. Klimov).

which then assemble into larger, channel-forming aggregates [24]. It appears that in general Aβ interactions with the lipid bilayer do not noticeably facilitate water permeation through the membrane [21,23].

Although the studies cited above provide important insights into the mechanism of Aβ-bilayer interactions, it is important to verify their conclusions using simulated tempering methods, such as replica exchange molecular dynamics (REMD). Two very recent studies have applied REMD to the problem of peptide–membrane interactions. Sugita and coworkers have used surface-tension (NPγT) REMD to study the structure of POPC bilayer and its interactions with WALP23 peptide [25]. They showed that NPγT REMD significantly enriches conformational sampling of lipids and peptide. In our previous study we have applied isobaric–isothermal (NPT) REMD to probe the interactions of Aβ10-40 monomer with zwitterionic DMPC bilayer [26]. We found that Aβ monomer binding to the DMPC bilayer causes dramatic structural transition in the peptide resulting in appearance of stable helix structure in the C-terminal. We have also determined that the central hydrophobic cluster and the C-terminal in Aβ not only govern binding to the bilayer, but also penetrate into the bilayer core. In contrast, the polar N-terminal and turn region form interactions mainly with the bilayer surface. Thus, in our previous study [26] we focused exclusively on the conformational changes in the binding Aβ peptide. However, based on the studies performed by other groups [19–21] we expect that binding and penetration of Aβ peptide into the bilayer may also perturb its structure. This specific issue, which was beyond the scope of our previous study [26], is addressed in this article.

Specifically, using NPT-REMD and all-atom explicit water model we study the structural changes in DMPC lipid bilayer caused by binding of Aβ monomer. As a control we use the MD simulations of Aβ-free DMPC bilayer. Our main results are as follows. First, Aβ peptide, which is bound and partially inserted in the bilayer, reduces the density of lipids in the binding "footprint" and indents the bilayer, thus creating a lipid density depression. Second, our simulations reveal thinning of the bilayer and a decrease in the area per lipid in the proximity of Aβ. Third, although the analysis of lipid hydrophobic core detects disordering in the orientation of lipid tails, it also shows surprisingly minor structural perturbations in the tail conformations. We explain these observations by shallow insertion of Aβ, which weakly affects the density of fatty acid tails beneath Aβ binding "footprint". Our fourth result suggests that partial insertion of Aβ monomer does not enhance water permeation through the DMPC bilayer and even causes significant dehydration of the lipid–water interface. We conclude the paper by comparing our results with previous studies and discussing their possible implications for Aβ cytotoxic mechanism.

2. Methods

2.1. All-atom explicit solvent model

We have performed two sets of simulations of the dimyristoyl-phosphatidylcholine (DMPC) lipid bilayer in explicit water, one with Aβ monomers interacting with the bilayer and another with the pure bilayer without peptides. We have selected DMPC lipids, because they are ubiquitous in cell membranes, small in size, and their structural and physicochemical properties are well known (Fig. 1a) [27]. In our simulations CHARMM22 protein force field with CMAP corrections [28] and the CHARMM36 lipid force field [29] were used. CMAP corrections are necessary to improve the agreement between experimental and in silico protein structures in the disordered regions [28]. To remain consistent with our previous studies [26,30,31], we used the amino-truncated Aβ10-40 peptide. It is important to note that the truncation of polar amino terminal increases the overall hydrophobicity of Aβ peptide that in turn may enhance its affinity with respect to binding to lipid bilayers.

Because the full description of Aβ + bilayer system can be found in our previous study [26], we provide only its brief summary below.

We considered two Aβ10-40 monomers interacting with the bilayer formed by 98 DMPC lipids (Fig. 1b). Each bilayer leaflet was composed of 49 lipids arranged in a 7×7 square shape. Aβ peptides were placed
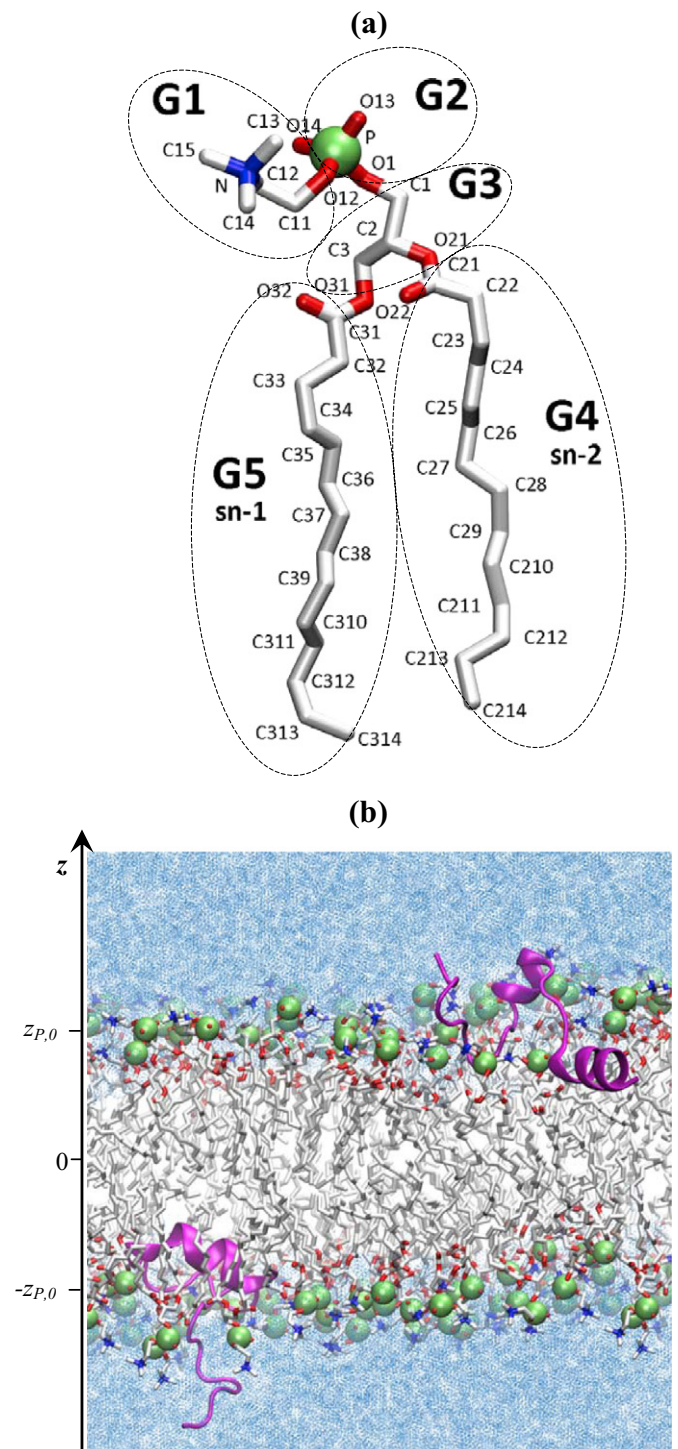
Fig. 1. (a) Chemical structure of DMPC lipid. Atom numbering follows that used in CHARMM36 force field. DMPC lipid is divided as marked into five groups: choline (G1), phosphate (G2), glycerol (G3), and two fatty acid tails (G4 and G5). Fatty acid chains sn-1 and sn-2 are also identified. (b) REMD simulation snapshot at 330 K illustrating binding of Aβ monomers to DMPC bilayer consisting of 98 lipids. The simulation system includes two Aβ monomers, which bind independently to the opposite leaflets of the bilayer. Lipid phosphorus atoms are in green, whereas Aβ peptides are shown in cartoon representation in purple. Water molecules are given by thin blue lines. The centers of mass of phosphorus atoms in each leaflet fluctuate around the positions $\pm z_{P,0}$ along the z-axis.

on the opposite sides of the bilayer. $A\beta$ protonation state corresponded to normal pH, and the peptides were capped with neutral acetylated and aminated terminals. To neutralize the system two sodium ions were added. Initial dimensions of the $A\beta$ + bilayer system were 55.6 Å × 55.6 Å × 81.4 Å, and it contained 4356 TIP3P water molecules. $A\beta$-free system included only the DMPC solvated bilayer and served as a control. Similar to $A\beta$ + bilayer system it contained 98 DMPC lipids arranged in a 7 × 7 square shape. Initial size of the simulation box was 56.2 Å × 56.2 Å × 60.0 Å, which contained 1743 TIP3P water molecules.

Following our previous study [26] simulation systems utilized two sets of constraints. The first applied harmonic potentials to the centers of mass of phosphorus (P) atoms in each leaflet. Specifically, this constraint used the force constant $k = 6.5 kcal/\left(mol Å^2\right)$ to approximately fix the center of mass of P atoms in each leaflet at the distance $|z_{P,0}| = 1$ 7.35 Å from the bilayer midplane (Fig. 1b). Because the constraint potentials act upon the centers of mass of P atoms rather than on individual atoms, they do not restrain the shape of the bilayer including its bending or indentation. The purpose of these constraints was to prevent disintegration of the lipid bilayer at high REMD temperatures (see below). These constraints were used in $A\beta$ + bilayer and $A\beta$-free systems. The second set of constraints applied only in $A\beta$ + bilayer system prohibited $A\beta$ peptides from crossing the periodic boundaries along the z dimension. These constraints were implemented as a pair of repulsive harmonic potentials with the force constant $k = 10 kcal/\left(mol Å^2\right)$, which act upon the z coordinates of peptide atoms (or ions) when their z is within 4 Å from the periodic boundary. These boundary constraints only affected peptide atoms or ions and were not applied to either lipid or water atoms. Their sole purpose was to block the aggregation of $A\beta$ peptides across periodic images.

To assess the impact of the constraints affecting phosphorus atoms, we have performed additional simulations of $A\beta$-free system, which did not include these constraints (see Supplementary Data).

2.2. Molecular dynamics simulations

Molecular dynamics (MD) simulations of all systems were performed using the isobaric–isothermal (NPT) ensemble and NAMD program [32]. Temperature was held constant using underdamped Langevin dynamics of "virtual" solvent with the damping coefficient $\gamma = 5 ps^{-1}$. Pressure was controlled by the Nose–Hoover Langevin piston method and a semi-isotropic pressure coupling scheme was applied, in which x and y box dimensions (in the bilayer plane) were coupled, whereas z dimension was adjusted independently. The Langevin piston period was set to 200 fs and the piston decay time was 100 fs. The integration step was set to 1 fs. All simulation systems utilized periodic boundary conditions. Electrostatic interactions were computed using Ewald summation, whereas van der Waals interactions were smoothly switched off in the interval from 8 to 12 Å. Covalent bonds were constrained by the SHAKE algorithm.

$A\beta$-free DMPC bilayer systems utilized conventional MD. In these systems temperature and pressure were held constant at 330 K and 1 atm. For $A\beta$-free system with the constraints four independent MD trajectories were produced, generating a total simulation time of 400 ns. Because 10 ns were discarded from the beginning of each trajectory as unequilibrated, the simulation time was reduced to 360 ns. Similarly, for $A\beta$-free system without the constraints two 60 ns trajectories were produced, from which 100 ns were used for analysis.

2.3. Replica exchange protocol

Due to the presence of peptides in $A\beta$ + bilayer system, enhanced conformational sampling, such as replica exchange molecular dynamics (REMD) [33,34], is necessary to achieve simulation convergence. REMD method must be adapted for isobaric–isothermal (NPT) ensemble, which is suitable for bilayers. NPT-REMD formalism is described in detail elsewhere [26,35]. In the REMD simulations of $A\beta$ + bilayer system, which were performed in our previous study [26], we have considered $R = 40$ replicas distributed exponentially in the temperature range from 320 to 430 K. The selection of slightly elevated temperature range facilitates conformational sampling. Pressure in all replicas was maintained at the constant value of $P = 1$ atm. Exchanges were attempted every 2 ps between all neighboring replicas along the temperature scale generating an average acceptance rate of 24%. Five independent REMD trajectories were generated, resulting in the cumulative simulation time of 4 μs or 100 ns per replica. The initial unequilibrated portions of the simulations were discarded, reducing the cumulative simulation time to 3.3 μs. However, use of two peptides independently interacting with the bilayer effectively doubles the cumulative simulation time per peptide to 6.6 μs. Analysis of REMD convergence and definitions of errors are presented in our previous work [26] and are also discussed in the Supplementary Data. These results demonstrate that REMD simulations approximately converge justifying the choice of REMD temperature range.

2.4. Computation of structural probes

To explore spatial distribution of atoms we computed the number densities $n = N/V$, where N is the number of atoms in the volume V. More specifically, we defined the atom number density $n(z)$ at the distance z from bilayer midplane as an average number of atoms in the narrow volume layer $(z, z + \Delta z)$, where $\Delta z = 0.5$ Å. Three such number densities, $n_l(z)$, $n_p(z)$, and $n_w(z)$, were computed for lipid, protein, and water heavy atoms, respectively. To characterize the distribution of lipids on the bilayer surface we used the area number density $n_P(x, y)$ defined as the average number of phosphorus atoms P in the area element $\Delta x \Delta y$ with the coordinates (x, y) $(\Delta x = \Delta y = 1$ Å$)$. In computing $n_P(x, y)$ the point $(0, 0)$ was always associated with the center of mass of $A\beta$ peptide. In addition, we have used the radial area number density $n_P(r)$ defined as the number of phosphorus atoms in the area enclosed by the concentric circles $(r, r + \Delta r)$, where $\Delta r = 0.5$ Å and r is the distance to the peptide center of mass. Finally, we computed the lipid atom number density $n_l(r, z)$ as a function of the distance to the peptide center of mass r and the distance to the bilayer midplane z. In these computations $n_l(r, z)$ reports the average number of lipid heavy atoms in the concentric circular layer of the width Δr and the thickness Δz at the distances r and z. The water atom number density $n_w(r, z)$ was defined in a similar way. Finally, we defined the radial distribution function $g_{PP}(r)$, which gives the average area number density of phosphorus atoms P at the distance r from a reference P. In the functions defined above the distance r between lipids (or water) and peptide was computed in (x, y) plane, i.e., in two dimensions with the coordinate z not included.

Area per lipid A_l was computed using Voronoi tessellation by applying Qhull program [36]. Phosphorus atoms were assumed to represent lipids, whereas the peptide was represented by the centers of mass of amino acid side chains. It is worth noting that the use of lipid centers of mass in tessellation does not lead to qualitatively different results. To exclude unbound amino acids a side chain was considered for Voronoi tessellation only if its center of mass occurred in the interval $0 < |z| < z_{P,0} + 6.5$ Å, where $z = 0$ Å corresponds to the bilayer midplane and $z_{P,0}$ is the average position of the center of mass of phosphorus atoms in a leaflet.

To quantify ordering of lipid molecules we used a generic order parameter

$$S = \frac{3cos^2\theta - 1}{2}, \tag{1}$$

where θ is the angle between a lipid vector and the bilayer normal. If lipid vectors are associated with the fatty acid C–H bonds, then Eq. (1) defines the lipid carbon–deuterium order parameter S_{CD},

which measures ordering of fatty acid tails sn-1 and sn-2 (Fig. 1a) with respect to the bilayer normal. If lipid vectors are represented by $C_{i-1} - C_i$ backbone bonds in fatty acid tails, then the same equation defines the order parameter S_{CC}, which provides additional measure of the orientation of fatty acid backbones with respect to bilayer normal. Ordering of lipid headgroups was assessed by $^{13}C - ^{31}P$ dipolar couplings [37,38]

$$\Delta v_D = 12236.5 \left| \frac{3cos^2\theta - 1}{2r^3} \right|. \tag{2}$$

In this equation θ is the angle between a C–P vector, defined by a given carbon atom C and phosphorus atom P, and the bilayer normal

and r is the distance between the atoms C and P. The parameter Δv_D was computed for all carbons in the lipid headgroup, glycerol, and six carbons from fatty acid tails, CX1, CX2, and CX14 (X = 2,3; Fig. 1a).

Additional measures of fatty acid conformations were provided by the number of gauche defects, fatty acid chain length, and tilt angle. To compute the number of gauche defects per fatty acid chain g we used the fatty acid backbone dihedral angles α defined by the carbons C_i, C_{i+1}, C_{i+2}, and C_{i+3}. For each fatty acid chain we can determine 11 such dihedral angles. Then, g is the number of these dihedral angles occurring in the intervals $[-120°, 0°]$ or $[0°, 120°]$. Fatty acid chain length L was defined as the distance between the carbonyl atom and the last carbon atom in a fatty acid chain. Tilt angle γ was computed as the angle between the vector $\overrightarrow{L}$ and the bilayer normal. Finally, we assumed that amino acid forms a contact with a lipid if the centers of mass of its side chain and any of the lipid structural groups are less than 6.5 Å apart.

For Aβ + bilayer system thermodynamic averages of structural quantities (denoted as < ... >) were computed using the multiple histogram method [39] adapted for NPT simulations [40,41]. Results are reported at $T = 330 K$ to maintain consistency with our previous studies [26,30]. Data from Aβ-free systems are presented as time averages obtained with an interval of 10 ps between structures. Due to the systems' symmetry with respect to the bilayer midplane and because in Aβ + bilayer system the peptides do not interact, all structural quantities were averaged over two leaflets.

### 2.5. Testing lipid force field and simulation design

To validate the selection of CHARMM36 lipid force field, we compared the lipid conformations sampled in Aβ-free system against experimental data [27,38,42]. To this end, we analyzed several structural quantities, such as area per lipid A_l, order parameter S_{CD}, dipolar coupling Δv_D, and the number of gauche defects g. The detailed comparison presented in Supplementary Data indicates that our simulations of the DMPC bilayer adequately reproduce experimental properties.

In Supplementary Data we also present the comparison of lipid conformations sampled in Aβ-free simulations with and without the constraints applied to the centers of mass of phosphorus atoms in each leaflet. The analysis suggests that these constraints do not appreciably affect lipid structure. This is not surprising, because when applied to the centers of mass of P atoms the constraints do not preclude bending or indentation of the bilayer. For brevity Aβ-free simulations with the constraints are referred to below as Aβ-free simulations or Aβ-free bilayer.

3. Results

3.1. Aβ impact on bilayer structure

Due to exhaustive sampling NPT-REMD allows us to examine in detail the impact of Aβ monomer on DMPC bilayer. In Aβ + bilayer simulations Aβ monomer binds to the bilayer with the probability $P_b \approx 1.0$, where P_b is the probability that at least one amino acid is bound [26]. According to our previous study binding of Aβ leads to shallow insertion of the peptide C-terminal and central hydrophobic cluster into the bilayer. To visualize the impact of Aβ insertion on the bilayer structure we first computed the area number density for lipid phosphorus atoms $n_P(x, y)$ (see Methods). Fig. 2a reveals that the peptide inflicts a striking density depression of phosphorus atoms, which becomes most pronounced in its center. The boundary of depression approximately occurs at the distance $R_c = 14 Å$ from the peptide center of mass, at which the number of peptide–lipid contacts reach maximum. Therefore, R_c can be considered as a radius of the peptide binding "footprint" on the DMPC bilayer. The lipids within the "footprint" are classified as proximal, whereas the lipids


(a)

(b)
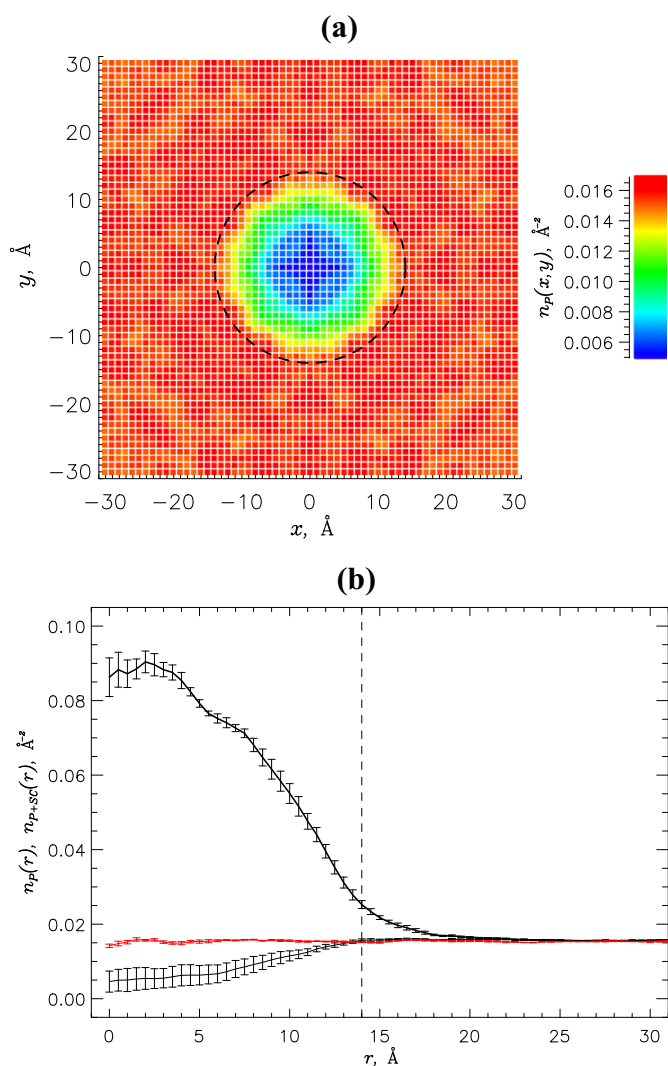
Fig. 2. (a) The area number density for lipid phosphorus atoms $n_P(x, y)$ on the bilayer surface as a function of coordinates x and y. The center of mass of Aβ peptide is placed at $x = 0$ Å and $y = 0$ Å. The density map is averaged over two Aβ peptides. Because $n_P(x, y)$ is intrinsically isotropic, the density map is further smoothed by averaging over the quadrants and the diagonals within the quadrants. The lipid density is color coded according to the scale. (b) Radial area number density of phosphorus atoms $n_P(r)$ with respect to the distance r from the peptide center of mass. The REMD data from Aβ + bilayer system are given in black, whereas the data from the control Aβ-free simulations are in red. Thick black line corresponds to the area number density $n_{P+sc}(r)$ combining phosphorus atoms with amino acid centers of mass. Errors are presented as bars. Both panels indicate that Aβ monomer creates a lipid density depression with the radius $R_c = 14 Å$ enclosed by dashed lines. Panel (b) also shows that the total number density within Aβ "footprint" is increased compared to Aβ-free regions (large r).

located outside the "footprint" are referred to as distant.[1] Further information is provided in Fig. 2b, which plots the radial area number density $n_P(r)$ with respect to the distance r from the peptide center of mass (see Methods). It is clear that within the peptide "footprint" one can distinguish two regions, where the density increases slowly ($r \lesssim 6\,\text{Å}$) and rapidly ($6\,\text{Å} \lesssim r < R_c$). The third region corresponds to distant lipids ($R_c < r$). From $A\beta$ + bilayer simulations the averages of n_P in the three regions are 0.006 ± 0.003, 0.011 ± 0.001, and $0.016 \pm 0.000\,\text{Å}^{-2}$, respectively. Therefore, these estimates and Fig. 2b imply that the area lipid density in the center of the "footprint" drops three times compared to the density in distant regions. Although lipid density drastically decreases within the "footprint", it remains far from being negligible ($n_P(r) \gtrsim 0.005\,\text{Å}^{-2}$). Additionally, Fig. 2b shows the area number density $n_{P+SC}(r)$ combining phosphorus atoms and the centers of mass of $A\beta$ side chains. The plot of $n_{P+SC}(r)$ reveals highly elevated number density at $r < R_c$ indicating that in the center of the binding "footprint" amino acids are mixed with the lipids. For example, in the distant regions ($r > R_c$) the average value of $n_{P+SC}(r)$ is $0.017 \pm 0.000\,\text{Å}^{-2}$, but it rises four-fold to $0.068 \pm 0.001\,\text{Å}^{-2}$ in the $A\beta$ "footprint" ($r < R_c$). Finally, Fig. 2b compares $n_P(r)$ computed for $A\beta$ + bilayer system with that obtained for $A\beta$-free bilayer. For both systems the area number densities at the distances $r > R_c$ coincide suggesting that the distant lipids in $A\beta +$ bilayer system have similar properties to those in $A\beta$-free bilayer.

The analysis above describes the distribution of lipids on the bilayer surface. In order to probe the distribution of lipid, water, and protein atoms across the bilayer we computed the atom number densities $n(z)$ at the distance z from bilayer midplane (see Methods). Fig. 3a compares these density profiles obtained near the bound peptide ($r < R_c$) and away from the peptide ($r > R_c$). For these comparisons we assume that the bilayer-water boundary in the distant regions ($r > R_c$) occurs at $z_b \approx 20.0\,\text{Å}$, where $n_l(z_b) \approx n_w(z_b)$. Consistent with Fig. 2 this figure demonstrates a considerable decrease in the density of proximal lipids ($r < R_c$). Specifically, when averaged over $0 < z < z_b$ the proximal lipid atom number density n_l^{prox} is reduced to $0.71 n_l^{dist}$, where n_l^{dist} is the density for distant lipids ($r > R_c$). In other words, below the peptide "footprint" the lipid atom number density is reduced, on an average, by about 30%. It is also worth noting that in Fig. 3a the maximum in peptide atom number density $n_p(z)$ at $z = 13\,\text{Å}$ approximately coincides with the maximum difference between $n_l^{prox}(z)$ and $n_l^{dist}(z)$. The impact of bound $A\beta$ peptide on individual lipid groups (see Fig. 1a) is illustrated in Fig. 3b. It follows from this figure and Table 1 that below the peptide "footprint" the atom number density for all groups G1–G5 is suppressed, from 25% for fatty acid chains (G4,G5) to 37% for phosphorus (G2). Furthermore, according to Table 1 the peaks in atom number densities $n_l(z; k)$ for all groups $k = $ G1–G5 in proximal lipids are shifted closer to the bilayer midplane by as much as $1.5\,\text{Å}$. These findings suggest that, although bound $A\beta$ peptide depresses the density of lipids through the leaflet volume, it produces the strongest impact on the lipid headgroups and glycerol, whereas the fatty acid tails residing deeper in the bilayer core experience weaker perturbation. In addition, we conclude that $A\beta$ not only creates a lipid density depression, but also indents the bilayer.

To directly probe bilayer indentation we defined the quantity $< z_P(r) >$, which is the average position along the axis z of phosphorus atoms at the distance r from the peptide center of mass. According to Fig. 4 $< z_P(r) >$ monotonically decreases as r becomes smaller. For example, the average $< z_P >$ for $r < 6\,\text{Å}$ is $15.3 \pm 0.6\,\text{Å}$, whereas at $r > R_c < z_P >= 17.4 \pm 0.1\,\text{Å}$. The latter agrees well with the value computed for $A\beta$-free system ($17.4 \pm 0.0\,\text{Å}$). Therefore, compared to the regions distant from $A\beta$ the bilayer is indented near the center of $A\beta$ "footprint" by $2.1\,\text{Å}$. On the other hand, the bilayer thickness away from $A\beta$ is not

(a)

(b)
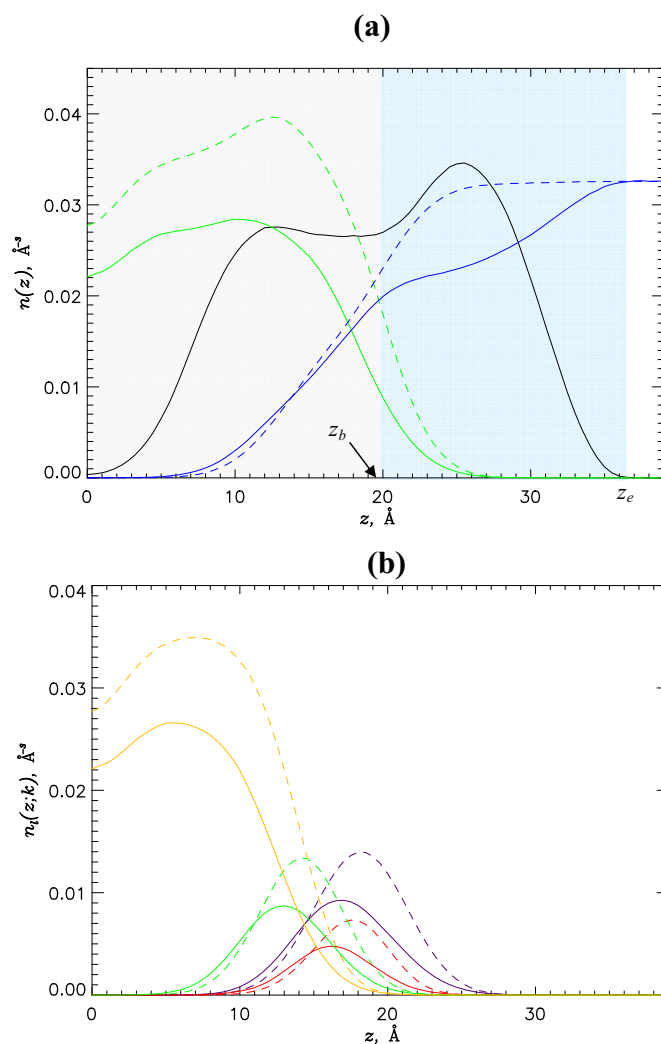
Fig. 3. (a) Heavy atom number densities as a function of the distance z from the bilayer midplane: lipid atom number density $n_l(z)$ is shown in green, water atom number density $n_w(z)$ is given in blue, and the peptide atom number density $n_p(z)$ is in black. To improve readability of the plot $n_p(z)$ is scaled by a factor of 10. Light gray and blue regions along z correspond to bilayer interior ($z < z_b$) and bilayer–water interface layer ($z_b < z < z_e$). (b) Heavy atom number densities $n_l(z; k)$ for lipid groups k ($=$G1–G5 in Fig. 1a) as a function of the distance z from bilayer midplane. Data in purple, red, green, and yellow correspond to choline (G1), phosphorus (G2), glycerol (G3), and fatty acid (G4, G5) groups. Solid and dashed lines represent the distributions computed for proximal and distant (with respect to $A\beta$ location) molecules, respectively. The figure shows that bound $A\beta$ reduces lipid density within its "footprint", indents the bilayer, and causes significant dehydration of its surface.

affected. In the Discussion we examine other estimates of bilayer thickness.

An important question pertains to the effect of $A\beta$ binding on lipid-lipid interactions. To answer this question we plot in Fig. 5 the radial
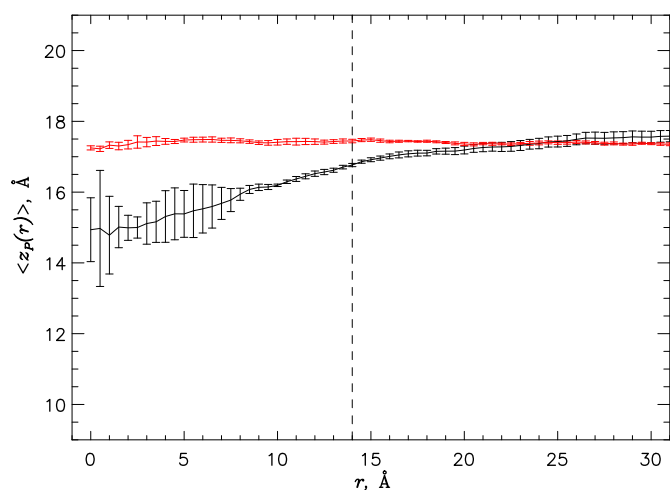
Table 1
Impact of $A\beta$ binding on lipid structural groups.

Lipid group, k	$n_l^{prox}(k)/n_l^{dist}(k)$[a]	$\Delta z_{max}(k)$, Å[b]
G1	0.66 ± 0.09	-1.0 ± 0.4
G2	0.63 ± 0.10	-1.5 ± 0.4
G3	0.65 ± 0.10	-1.0 ± 0.5
G4/G5	0.75 ± 0.09	-1.5 ± 0.3

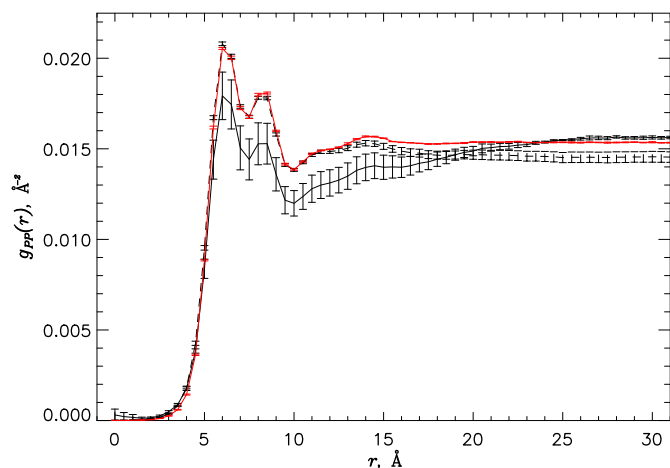[a] densities are averaged over $0 < z < z_b$.
[b] $\Delta z_{max}(k) = z_{max}^{prox}(k) - z_{max}^{dist}(k)$, where $z_{max}(k)$ are the locations of maxima in $n_l(z; k)$.

---

[1] Unless otherwise noted lipid position is represented by its center of mass.

Fig. 4. Bilayer indentation $<z_P(r)>$ as a function of the distance r from the center of mass of bound Aβ monomer. The REMD data for Aβ + bilayer system are given in black, whereas the data from the control Aβ-free simulations are in red. Errors are presented as bars. Vertical black dashed line shows the depression radius $R_c = 14$ A$^\circ$. The figure suggests that binding of Aβ monomer causes DMPC bilayer thinning.

distribution function for phosphorus atoms $g_{PP}(r)$ computed separately for proximal and distant lipids (see Methods). This figure shows that, although at $r\lesssim20$ A$^\circ$ $g_{PP}(r)$ for proximal lipids is consistently smaller than for distant lipids, the shapes of both functions are remarkably similar. For example, the peaks at $r_{fs} = 6$ A$^\circ$ in both $g_{PP}(r)$ functions correspond to the first shell of lipids surrounding a reference lipid. Smaller values of $g_{PP}(r)$ for proximal lipids indicate that the local density of phosphorus atoms is reduced near the bound Aβ that is consistent with the conclusions drawn from Figs. 2 and 3. In addition, Fig. 5 presents $g_{PP}(r)$ function computed for Aβ-free bilayer, which demonstrates remarkable agreement with $g_{PP}(r)$ obtained for distant lipids up to the distance $r\approx$ 10 A$^\circ$. Discrepancies between $g_{PP}(r)$ for Aβ-free bilayer and for distant lipids at $r>10$ A$^\circ$ reflect the influence of lipid density depression created by the peptide in the Aβ + bilayer system. Thus, the results presented in Fig. 5 suggests that (i) the local packing of distant lipids is not affected by Aβ, and (ii) the packing of proximal lipids is reduced, because there are fewer neighboring lipids surrounding proximal lipids. Given the similarity in $g_{PP}(r)$ shape between proximal and distant lipids and the

fact that the first lipid shell is located at the same distance r_{fs}, we conclude that Aβ binding does not significantly affect lipid–lipid interactions.

Further information about the impact of bound Aβ on lipid bilayer is provided by the area per lipid A_l, a quantity frequently used in membrane simulations. Specifically, we computed the area per lipid $<A_l(r)>$ as a function of the distance from the peptide center of mass r. Fig. 6 demonstrates that the areas per proximal lipids ($r < R_c$) are dramatically lower than for distant lipids ($r > R_c$). Indeed, the corresponding averages of $<A_l(r)>$ are 42.8 ± 1.5 and 61.8 ± 0.5 Å^2. If we restrict the computations to the center of the binding "footprint" ($r<6$ A$^\circ$) and to "very" distant lipids ($r>20$ A$^\circ$), then $<A_l>$ become 33.9 ± 3.2 and 63.5 ± 0.4 Å^2, respectively. In contrast, the area per distant lipids ($r>20$ A$^\circ$) is not affected by Aβ monomer, because its value is close to $<A_l>$ computed for Aβ-free system (65.1 ± 0.00 Å^2).

3.2. Aβ impact on the structure of lipid molecules

In this section we explore the impact of Aβ binding on the conformations and orientation of lipid molecules. To this end, we first present in Fig. 7a the lipid carbon–deuterium order parameter $- <S_{CD}(i)>$ for each carbon i in the fatty acid chain sn-2. As in the analysis above $<S_{CD}(i)>$ is computed separately for proximal and distant lipids. The figure shows that the order parameter of proximal lipids is consistently lower than the order parameter of distant lipids indicating that the former are more disordered. Indeed, the average value of $- <S_{CD}(i)>$ for 13 carbons in proximal lipids is 0.13 ± 0.00, but it increases to 0.16 ± 0.00 when distant lipids are considered. Furthermore, $<S_{CD}(i)>$ distributions observed for distant lipids and obtained for Aβ-free bilayer are in good agreement, e.g., the root mean square deviation (RMSD) between them is just 0.005. For comparison, the RMSD between proximal lipids and the lipids from Aβ-free system is 0.029, which is almost six-fold higher. In Fig. S6 from Supplementary Data we provide an additional plot of $- <S_{CD}(r; i)>$, which shows the order parameter dependence on the distance r from the peptide center of mass. Fig. S6 demonstrates that the disorder in fatty acid chains monotonically grows as the distance to the peptide decreases. Similar results have been obtained for sn-1 chains. For example, for proximal and distant
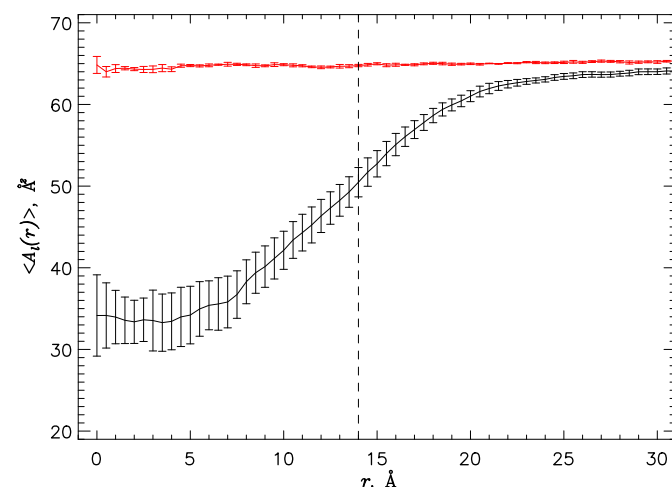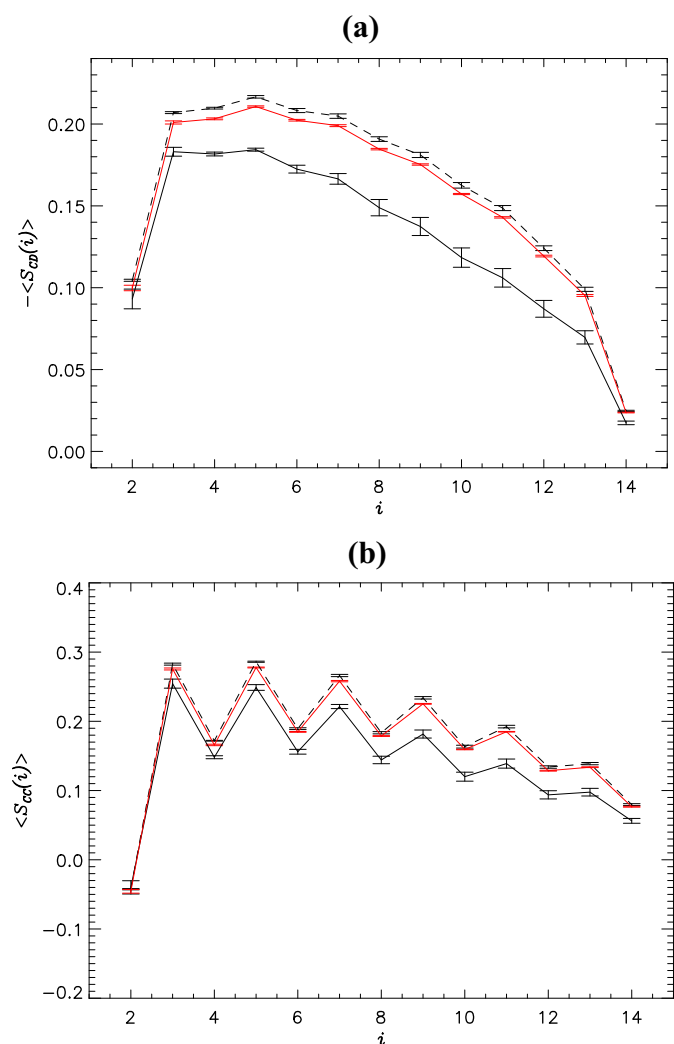

Fig. 5. The radial number density distribution function for phosphorus atoms $g_{PP}(r)$ as a function of the distance r from a reference phosphorus atom. The REMD data for Aβ + bilayer system and the data from the control Aβ-free simulations are in black and red, respectively. Solid and dashed lines represent the distributions computed for proximal and distant (with respect to Aβ) reference lipids. Bars indicate errors. The figure suggests that Aβ binding does not change lipid–lipid interactions, but reduces their surface density.

Fig. 6. Area per lipid $<A_l(r)>$ computed as a function of a distance r to Aβ monomer center of mass. The REMD data for Aβ + bilayer system and the data from the control Aβ-free simulations are in black and red, respectively. Errors are shown as bars. Vertical black dashed line shows the depression radius $R_c = 14$ A$^\circ$. The figure shows a dramatic decrease in the area per lipid in the vicinity of the bound peptide.

lipids the average values of $-<S_{CD}(i)>$ are 0.12 ± 0.00 and 0.16 ± 0.00.

From the analysis of $<S_{CD}(i)>$ alone it is unclear if the disordering effect is limited to the orientation of C−H bonds or it also impacts the fatty acid backbone. To probe the orientation of fatty acid tails with respect to bilayer normal, we used the order parameter $<S_{CC}(i)>$ (see Methods and Fig. 7b). This figure indicates that Aβ binding also disorders orientations of fatty acid tails. Indeed, the RMSD between $<S_{CC}(i)>$ obtained for distant lipids and those found in Aβ-free bilayer is 0.006, but it grows five-fold to 0.032, if proximal lipids are compared against those in Aβ-free bilayer. The average $<S_{CC}(i)>$ for 13 carbons in proximal and distant lipids are 0.14 ± 0.00 and 0.18 ± 0.00, respectively. Because both order parameters, $<S_{CD}(i)>$ and $<S_{CC}(i)>$, are reduced for proximal lipids compared to distant ones, we conclude that Aβ binding disorders fatty acid tails. It is also evident that Aβ binding does not impact fatty acid tails in distant lipids. Similar conclusions follow from the analysis of sn-1 chains.

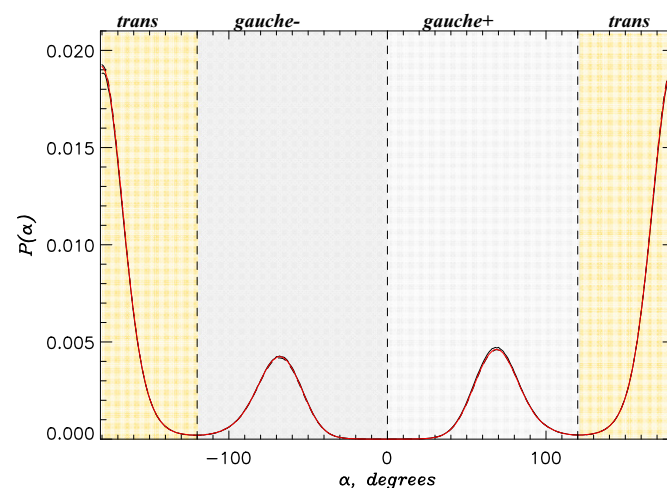It is important to note that disordering of fatty acid tails may occur, because Aβ induces conformational flexibility in the tails or because the tail orientations change. (The analysis below focuses on sn-2 chains, although similar results were obtained for sn-1 tails.) To distinguish between the two possibilities, we considered the number of gauche defects g in fatty acid backbones. Fig. 8 shows the probability distributions of dihedral angles α in the sn-2 fatty acid chains, $P(\alpha)$. Comparison of $P(\alpha)$ computed for proximal and distant lipids reveals that the distributions of dihedral angles in the fatty acid tails are not affected by Aβ. Specifically, the numbers of gauche defects g in proximal and distant lipids are about the same being equal to 3.7 ± 0.0 and 3.6 ± 0.0. Furthermore, the latter is equal to the value of g obtained from Aβ-free simulations (see Supplementary Data). Lipid tail structure can be further analyzed by plotting the probability distributions of the lengths of fatty acid sn-2 chains, $P(L)$ (Fig. 9a). The average chain lengths $<L>$ for proximal and distant lipids and for the lipids from Aβ-free bilayer are 13.3 ± 0.0, 13.5 ± 0.0, and 13.5 ± 0.0 Å, respectively. Consistent with the analysis of gauche defects these results show that Aβ does not appreciably affect the conformations of fatty acid tails. Finally, we present in Fig. 9b the probability distributions of fatty acid tilt angles $P(\gamma)$ for sn-2 chains (see Methods for γ definition). It follows from this figure that the average values of γ for proximal and distant lipids and for the lipids from Aβ-free bilayer are $144.8 \pm 0.4°$, $149.4 \pm 0.2°$, and $148.8 \pm 0.1°$, respectively. The analysis of the dependence of γ on the distance to the peptide r shows that within the center of Aβ "footprint" ($r<6\,Å$) the tilt is further increased to $141.4 \pm 2.8°$. These findings register larger tilt of proximal lipid tails compared to distant ones. Therefore, Figs. 8 and 9 suggest that Aβ binding leaves lipid conformations intact, but increases the tilt of fatty acid tails. The implication of these results is considered in the Discussion.

3.3. Impact of Aβ binding on water distribution

It is important to explore the effect of Aβ binding on the distribution of water near the DMPC bilayer and its permeation through the bilayer. Fig. 3a shows the water atom number density $n_w(z)$ computed separately for proximal ($r < R_c$) and distant ($r > R_c$) water molecules (r is

(a)

(b)

Fig. 7. (a) Lipid carbon–deuterium order parameter $-<S_{CD}(i)>$ computed for carbon atoms i in the fatty acid chains sn-2. (b) Complementary order parameter $<S_{CC}(i)>$ computed for carbon atoms i in the fatty acid chains sn-2. The parameter S_{CD} probes the orientation of carbon−hydrogen bonds with respect to the bilayer normal, whereas S_{CC} reports the orientation of the fatty acid backbone bonds with respect to the bilayer normal. REMD data for Aβ+bilayer system and the data from the control Aβ-free simulations are in black and red, respectively. Solid and dashed lines represent proximal and distant (with respect to Aβ) lipids. Bars indicate errors. Both panels suggest that Aβ peptide disorders the orientation of lipid tails with respect to the bilayer normal.

Fig. 8. Probability distributions $P(\alpha)$ of backbone dihedral angles α in the sn-2 fatty acid chains. REMD data for Aβ+bilayer system and the data from the control Aβ-free simulations are in black and red, respectively. Solid and dashed lines represent proximal and distant (with respect to Aβ) lipids. Yellow, dark and light gray regions correspond to *trans*, *gauche-*, and *gauche+* states, respectively, whereas the vertical black dashed lines show the boundaries of these regions. As three sets of data in the plot virtually coincide, it strikingly demonstrates that Aβ peptide bound to the bilayer does not change the conformations of lipid tails.

(a)

(b)
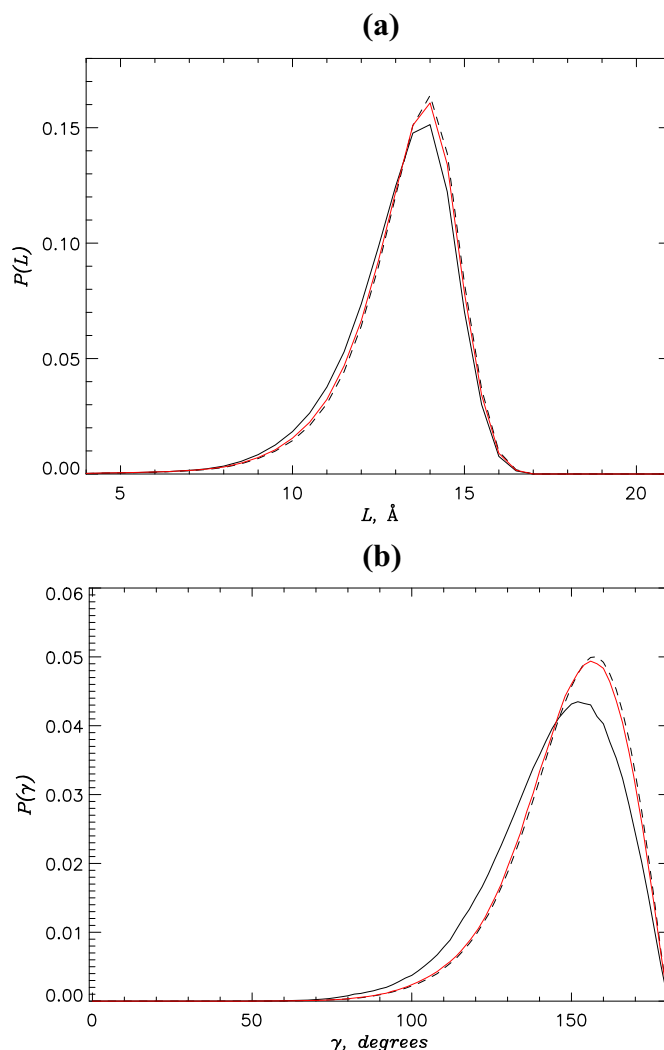
Fig. 9. (a) Probability distributions $P(L)$ of end-to-end lengths L for sn-2 chains. (b) Probability distributions $P(\gamma)$ of fatty acid tilt angles γ for sn-2 chains. REMD data for Aβ + bilayer system and the data from the control Aβ-free simulations are in black and red, respectively. Solid and dashed lines represent proximal and distant (with respect to Aβ) lipids. The figure suggests that while binding of Aβ does not change the end-to-end length of fatty acid tails, it increases their tilt with respect to the bilayer normal.

the distance to Aβ center of mass). It follows from this figure that inside the bilayer ($z < z_b$) no significant changes in the water density are observed between the distant and proximal regions, i.e., $n_w^{prox}(z < z_b) \approx n_w^{dist}(z < z_b)$. However, Fig. 3a indicates that Aβ peptide markedly reduces water density in the vicinity of the bilayer. To quantify this effect we define the interface water layer, which extends along the z-axis from the bilayer-water boundary at z_b to z_e, at which the influence of bilayer on water density vanishes ($n_w^{prox}(z_e) \approx n_w^{dist}(z_e)$). From the plots in Fig. 3a we find $z_e \approx 35.5\,\text{Å}$. By comparing water atom number densities averaged over the interface layers, which are proximal and distant from the bound Aβ, we determine that $n_w^{prox}(z_b < z < z_e) = 0.83 n_w^{dist}(z_b < z < z_e)$. If the same computations are restricted to the center of Aβ "footprint" ($r < 6\,\text{Å}$), then $n_w^{prox}(z_b < z < z_e)$ is further reduced to $0.70 n_w^{dist}(z_b < z < z_e)$. Interestingly, the analysis of Fig. 3a indicates that the maximum in the peptide atom number density $n_p(z)$ at $z = 25\,\text{Å} > z_b$ coincides with the maximum difference between $n_w^{prox}(z)$ and $n_w^{dist}(z)$ in the interface layer. Taken together, these observations argue that partial insertion of Aβ does not enhance water permeation into the bilayer within its "footprint". Furthermore, bound Aβ causes noticeable dehydration of the bilayer water interface by 20% within the peptide "footprint", which increases to 30% in the "footprint" center.

4. Discussion

4.1. Aβ perturbs and indents DMPC bilayer

We have used all-atom explicit water model and isobaric–isothermal REMD simulations to probe binding of Aβ monomers to DMPC bilayer. In the previous study we have found that binding of Aβ leads to shallow insertion of the peptide C-terminal and central hydrophobic cluster into the bilayer [26]. In this study, we have analyzed the impact of Aβ monomers in the structure of lipid bilayer. Our findings are as follows. First, Aβ causes a depression of lipid density on the bilayer surface, effectively creating a shallow hole within the bilayer structure. For example, lipid area density in the center of Aβ "footprint" drops three-fold compared to the density in Aβ-free regions. Second, Aβ indents the lipid bilayer by pushing lipids toward the bilayer midplane.

To provide visual illustration of these observations we present Fig. 10a which shows the number density of lipid heavy atoms $n_l(r, z)$ as a function of the distance to the peptide center of mass r and the distance to the bilayer midplane z. This plot together with the cartoon in Fig. 10b vividly illustrates the density depression caused by Aβ peptide in the upper bilayer leaflet. To quantify the effects of Aβ binding

(a)

(b)

(c)
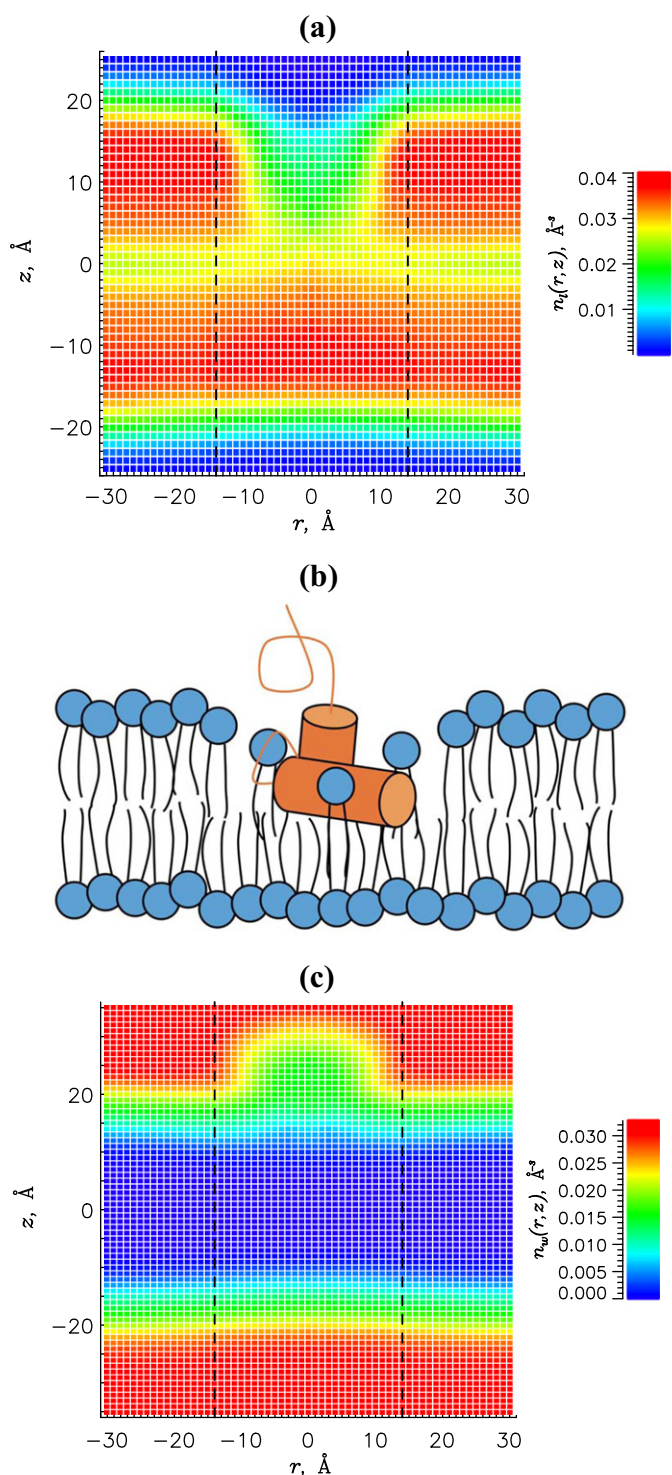
Fig. 10. (a) The number density of lipid heavy atoms $n_l(r, z)$ computed as a function of the distance r to Aβ center of mass and the position z along the bilayer normal. (b) A schematic cartoon summarizing lipid density depression caused by binding Aβ monomer. Lipid headgroups are shown in blue, whereas Aβ helices are represented by orange cylinders. (c) The number density of water oxygen atoms $n_w(r, z)$ computed as a function of the distance r to Aβ center of mass and the position z along the bilayer normal. In panels (a,c) the densities are color coded according to the scales on the right. The extent of lipid density depression with the radius $R_c = 14\,\text{Å}$ is shown by vertical dashed lines. Data presented in the panels (a,c) are averaged over two Aβ peptides. Panels (a–b) provide a vivid illustration of lipid density depression within the "footprint" of bound Aβ monomer. Panel (c) demonstrates a dehydration of DMPC bilayer caused by Aβ monomer.

we computed the average $n_l(r, z)$ for $r < R_c$ and $0 < z < z_b$ (z_b is the bilayer-water boundary defined in the Results) and found it to be equal to $0.026 \pm 0.002\,\text{Å}^{-3}$. The corresponding averages in the distant region of the upper leaflet ($r > R_c$, $0 < z < z_b$) and in the proximal region of the lower leaflet ($r < R_c$, $-z_b < z < 0$) are 0.034 ± 0.000 and $0.034 \pm 0.000\,\text{Å}^{-3}$, respectively. These values indicate that Aβ binding affects only the upper bilayer leaflet within the binding "footprint", whereas the lower leaflet remains largely unperturbed. Therefore, we surmise that shallow peptide insertion fails to disturb lipid structure throughout the bilayer cross-section as depicted in Fig. 10b. Importantly, Fig. 10a affords a direct estimate of bilayer thinning. For this purpose we redefine the bilayer boundary as $z_l(r)$, at which $n_l(r, z_l) = 0.5n_{l,max}(r)$ and $n_{l,max}(r)$ is the maximum of $n_l(r, z)$ at a given r. Because z_l is selected such that $z_l \approx z_b = 20.0\,\text{Å}$ at $r > R_c$, we can consider the bilayer boundary even in dehydrated regions within the binding "footprint", where z_b is ill-defined. Taking into account that the average z_l in the center of Aβ "footprint" ($r < 6\,\text{Å}$) is $13.8\,\text{Å}$, we conclude that Aβ indents the upper leaflet by 6.2 Å. Interestingly, according to Fig. 10a lipid density depression in the upper leaflet is mirrored by minor indentation in the lower leaflet. Using $-z_l(r)$ computed for the lower leaflet the amplitude of its indentation was found to be 1 Å. Thus, the actual thinning ΔD of the bilayer near Aβ binding location is about 7.2 Å. This estimate provides a better measure of bilayer thinning than the indentation amplitude based on the positions of phosphorus atoms in the upper leaflet alone.

Depression of lipid density and bilayer thinning raises the question about the effect of Aβ on lipid-lipid interactions. The radial distribution functions $g_{PP}(r)$ for lipid phosphorus atoms in Fig. 5 demonstrate that the distance between the reference lipid and the first lipid shell is the same ($r_{fs} = 6\,\text{Å}$) for proximal and distant lipids. Thus, although $g_{PP}(r)$ for proximal lipids is suppressed reflecting lipid density depression, the lipid–lipid interactions themselves are not affected by the peptide. It is also important to reconcile lipid density depression with the changes in area per lipid A_l, which is decreased almost two-fold (from 63.5 to 33.9 Å^2) in the center of Aβ binding "footprint". Using Fig. 2b we showed that within the peptide "footprint" lipids are mixed with amino acids resulting in overall denser molecular packing compared to distant regions. Specifically, we showed that the area number density combining lipid phosphorus atoms with side chain centers of mass increases four-fold within Aβ "footprint" compared to Aβ-free regions. To directly visualize this result we present in Fig. S7 from Supplementary Data a snapshot of Voronoi tessellation of bilayer surface from Aβ + bilayer simulations. The figure reveals that due to increased density the area of proximal lipid polygons is reduced compared to distant lipids. Therefore, the peptide "footprint" is more densely packed than Aβ-free regions that, in turn, explains a two-fold reduction in area per lipid A_l.

Because the impact of Aβ monomer on lipid sn-1 and sn-2 chains is quantitatively similar, we concentrated our analysis on sn-2 tails. Lipid order parameters $<S_{CD}>$ plotted in Fig. 7a indicate disordering of proximal lipids in comparison with distant lipids. We showed that average S_{CD} for distant lipids is 0.16, but for proximal lipids it decreases to 0.13. The distribution of $<S_{CD}(r; i)>$ presented in Fig. S6 further shows that lipid disordering begins with terminal carbons in the fatty acid sn-2 chains. The second lipid order parameter S_{CC} demonstrates that disordering in lipids is not limited to C–H bonds, but involves fatty acid tail backbones. Surprisingly, the analysis of the probability distributions of dihedral angles $P(\alpha)$ in the fatty acid tails and of their end-to-end lengths $P(L)$ indicates that Aβ does not perturb lipid conformations themselves. However, the probability distributions of tilt angles $P(\gamma)$ implicate a larger tilt (i.e., smaller γ) for proximal lipids with respect to bilayer normal. To check if the changes in tilt angle alone are sufficient to produce variations in S_{CD} observed in Fig. 7a we used the following procedure. Using Aβ-free simulations we tabulated the function $S_{CD}(\gamma; i)$ and then computed the average $S_{CD}(i)$ for each carbon i using the distributions $P(\gamma)$ for distant and proximal lipids in Fig. 9b.

The functions $S_{CD}(i)$ reconstructed through this procedure reproduce remarkably well the plots in Fig. 7a. Therefore, changes in the tilt of lipid tails are responsible for the differences in $< S_{CD}(i) >$ observed between proximal and distant lipids. This outcome is consistent with the observation made previously that variations in S_{CD} can be accounted by the lipid tilt [43]. Taken together these results imply that Aβ binding mainly disorders spacial orientation of fatty acid tails, while leaving their internal conformations fairly intact.

Using Fig. 3a we concluded that Aβ binding does not enhance water permeation into the bilayer. Furthermore, bound Aβ causes noticeable dehydration of the bilayer–water interface by 20% within the peptide "footprint" increasing to 30% in the "footprint" center. To visualize water distribution near the bilayer we plot in Fig. 10c the number density of water oxygen atoms $n_w(z, r)$. The plot shows a dehydrated region near the bilayer surface in the proximity of the bound Aβ. Therefore, Fig. 10c directly confirms that Aβ monomer dehydrates zwitterionic DMPC bilayer and does not enhance water permeation through the bilayer.

Finally, it is useful to discuss potential finite size effects in our simulations. We found that Aβ-free systems reasonably reproduce DMPC experimental measurements (see Supplementary Data). We have also shown that distant lipids have already the properties similar to those in Aβ-free systems. These two observations argue that the number of lipids in our systems appears sufficient.

4.2. Comparison with previous studies and implications for cytotoxicity

The impact of Aβ peptides on the structure of lipid bilayers has been considered in a number of previous studies, so it is important to compare our results with previous data. Using several structural measures we showed that binding of Aβ disorders the orientation of fatty acid tails. Similar conclusions have been reported in the molecular dynamics (MD) simulations of DPPC bilayers with embedded Aβ peptides [20,21]. Specifically, it was found that S_{CD} order parameter decreases in the close proximity of pre-inserted Aβ monomers and oligomers. Furthermore, around the embedded Aβ a noticeable thinning of the bilayer by as much as 10 Å was observed [20]. Recent MD work probing the effect of surface binding of Aβ monomer on POPC bilayer also found a decrease in the bilayer thickness, albeit by only 3 Å [19]. These observations are consistent with our results that partial insertion of Aβ monomer reduces the thickness of DMPC bilayer by $\Delta D = 7.2$ A$^\circ$ in the center of binding "footprint". Approximate agreement of our ΔD with previous simulation results alleviates the concern that the constraints utilized in our system could affect bilayer thickness. Previous and our simulation results support the view that bilayer thinning becomes more significant with deeper Aβ insertion into the bilayer [19]. Another quantity frequently analyzed in computational studies is the area per lipid A_l. Most previous studies have registered a decrease in A_l in the proximity of Aβ [20,21,23]. For example, for DPPC with embedded Aβ a more than 50% drop in the area per lipid (from 62 to 25A$^{\circ 2}$) was reported [20]. That result is similar to our finding for DMPC that Aβ binding induces a twofold decrease in A_l.

Although previous studies have observed perturbation in lipid structure caused by Aβ, they did not find that Aβ peptide enhances water permeation through the bilayer. For example, when Aβ is pulled deep into the DPPC bilayer, the peptide impedes water flux through the bilayer [23]. Another study has shown that Aβ monomers do not change water permeation compared to Aβ-free bilayers [21]. These results are in agreement with our findings that water permeation into the DMPC bilayer is not enhanced by shallow insertion of Aβ monomer and that bound Aβ dehydrates the bilayer surface.

Although the comparisons with experimental studies cannot be as direct as with previous simulations, they are important for judging the accuracy of computational predictions. Recent experiments have shown that the disruption of DOPC/POPG bilayers is more severe, when Aβ42 peptides are inserted rather than associated with the

membrane [15]. Similar result follows from the studies of Aβ binding to zwitterionic POPC bilayers [8]. This work showed that surface Aβ binding without penetration into the bilayer core does not change deuterium NMR spectra of fatty acids. These observations agree well with our conclusion that, while shallow insertion of Aβ monomer causes pronounced lipid density depression on the DMPC bilayer surface, it fails to significantly disorder bilayer hydrophobic core or the opposite leaflet. Experiments have also addressed the issue of membrane thinning [9]. Specifically, electron density profiles obtained from X-ray diffraction indicate that interaction of apparently soluble Aβ with cellular membrane reduces its thickness by about 6 Å. This estimate is in good agreement with our computational finding.

The comparisons presented above suggest that our results are consistent with previous computational and experimental investigations. We believe that our work takes the analysis of Aβ-bilayer interactions one step further by applying exhaustive conformational NPT-REMD sampling. Although computationally expensive, this method allowed us to construct an equilibrium density map of the DMPC bilayer revealing lipid density depression on its surface induced by Aβ monomer (Fig. 10a,b). Qualitative agreement of our predictions with previous studies employing different lipid bilayers, models, and sampling methods argues that the impact of Aβ monomer on the zwitterionic DMPC bilayer depicted by us may be generic. The main conclusion of our earlier study [26] was that binding of Aβ monomer to zwitterionic DMPC bilayer results in a shallow penetration of the peptide, mainly, of its C-terminal and central hydrophobic cluster, into the bilayer. Here, we showed that this mode of Aβ-bilayer interaction induces a strong density depression on the bilayer surface, but it fails to produce a pore across the bilayer. One may conjecture that the limited scope of structural perturbation of the zwitterionic bilayer caused by Aβ monomer represents the molecular basis of its low cytotoxicity.

5. Conclusions

We have used isobaric–isothermal replica exchange molecular dynamics to study the impact of Aβ monomer on the equilibrium properties of DMPC bilayer. Four main conclusions follow from this study. First, Aβ peptide, which according to our previous study is bound and partially inserted in the bilayer [26], reduces the density of lipids in the binding "footprint" and indents the bilayer, thus creating a lipid density depression. Second, our simulations reveal thinning of the bilayer and a decrease in the area per lipid in the proximity of Aβ monomer. Third, although the analysis of lipid hydrophobic core detects disordering in the orientations of lipid tails, it also shows surprisingly minor structural perturbations in the tail conformations. We explain these observation by shallow insertion of Aβ, which weakly affects the density of fatty acid tails beneath Aβ binding "footprint". Finally, shallow insertion of Aβ monomer does not enhance water permeation through the DMPC bilayer and even results in considerable dehydration of the bilayer–water interface. Therefore, our data imply that Aβ monomer bound to the surface of DMPC bilayer fails to perturb the bilayer structure across both leaflets. We propose that the limited scope of structural perturbations in the zwitterionic bilayer caused by Aβ monomer represents the molecular basis of its low cytotoxicity.

Appendix A. Supplementary data

Supplementary data to this article can be found online at http://dx.doi.org/10.1016/j.bbamem.2014.07.010.

References

[1] J. Hardy, D.J. Selkoe, The amyloid hypothesis of Alzheimer's disease: progress and problems on the road to therapeutics, Science 297 (2002) 353–356.

[2] C. Haass, M.G. Schlossmacher, A.Y. Hung, C. Vigo-Pelfrey, A. Mellon, B.L. Ostaszewski, I. Lieberburg, E.H. Koo, D. Schenk, D.B. Teplow, D.J. Selkoe, Amyloid β-peptide is produced by cultured cells during normal metabolism, Nature 359 (1992) 322–325.

[3] C. Haass, D.J. Selkoe, Soluble protein oligomers in neurodegeneration: lessons from the Alzheimer's amyloid β-peptide, Nat. Rev. Mol. Cell Biol. 8 (2007) 101–112.

[4] T.L. Williams, L.C. Serpell, Membrane and surface interactions of Alzheimer's Aβ peptide—insights into the mechanism of cytotoxicity, FEBS J. 278 (2011) 3905–3917.

[5] F.J. Sepulveda, J. Parodi, R.W. Peoples, C. Opazo, L.G. Aguayo, Synaptotoxicity of Alzheimer's beta amyloid can be explained by its membrane perforating property, PLoS One 5 (2010) e11820–e11829.

[6] S.R. Durell, H.R. Guy, N. Arispe, E. Rojas, H.B. Pollard, Theoretical models of the ion channel structure of amyloid β-protein, Biophys. J. 67 (1994) 2137–2145.

[7] N. Arispe, J.C. Diaz, O. Simakova, Aβ ion channels. Prospects for treating Alzheimer's disease with Aβ channel blockers, Biochim. Biophys. Acta 1768 (2007) 1952–1965.

[8] E. Terzi, G. Holzemann, J. Seelig, Interaction and Alzheimer's β-amyloid peptide(1–40) with lipid membranes, Biochemistry 36 (1997) 14845–14852.

[9] R.P. Mason, R.F. Jacob, M.F. Walter, P.E. Mason, N.A. Avdulov, S.V. Chochina, U. Igbavboa, W.G. Wood, Distribution and fluidizing action of soluble and aggregated amyloid β-peptide in rat synaptic plasma membranes, J. Biol. Chem. 274 (1999) 18801–18807.

[10] C. Yip, J. McLaurin, Amyloid-β peptide assembly: a critical step in fibrillogenesis and membrane disruption, Biophys. J. 80 (2001) 1359–1371.

[11] M. Bokvist, F. Lindstrom, A. Watts, G. Grobner, Two types of Alzheimer's β-amyloid (1–40) peptide membrane interactions: aggregation preventing transmembrane anchoring versus accelerated surface fibril formation, J. Mol. Biol. 335 (2004) 1039–1049.

[12] A. Qulst, I. Doudevski, H. Lin, R. Azimova, D. Ng, B. Franglone, B. Kagan, J. Ghiso, R. Lal, Amyloid ion channels: a common structural link for protein-misfolding disease, Proc. Natl. Acad. Sci. U. S. A. 102 (2005) 10427–10432.

[13] S. Nag, J. Chen, J. Irudayaraj, S. Maiti, Measurement of the attachment and assembly of small amyloid-β oligomers on live cell membranes at phsiological concentrations using single-molecule tools, Biophys. J. 99 (2010) 1969–1975.

[14] E.E. Ambroggio, D.H. Kim, F. Separovic, C.J. Barrow, K.J. Barnham, L.A. Bagatolli, G.D. Fidelio, Surface behavior and lipid interaction of Alzheimer's β-amyloid peptide 1–42: a membrane-disrupting peptide, Biophys. J. 88 (2005) 2706–2713.

[15] T.-L. Lau, E.E. Ambroggio, D.J. Tew, R. Cappai, C.L. Masters, G.D. Fidelio, K.J. Barnham, F. Separovic, Amyloid-β peptide disruption of lipid membranes and the effect of metal ions, J. Mol. Biol. 356 (2006) 759–770.

[16] P. Cizas, R. Budvytyte, R. Morkuniene, R. Modovan, M. Broccio, M. Lösche, G. Niaura, G. Valincius, V. Borutaite, Size-dependent neurotoxicity of β-amyloid oligomers, Arch. Biochem. Biophys. 496 (2010) 84–92.

[17] J.J. Kremer, R.M. Murphy, Kinetics of adsorption of β-amyloid peptide Aβ(1–40) to lipid bilayers, J. Biochem. Biophys. Methods 57 (2003) 159–169.

[18] Y. Nakazawa, Y. Suzuki, M. Williamson, H. Saito, T. Asakura, The interaction of amyloid Aβ(1–40) with lipid bilayers ganglioside as studied by P[31] solid state NMR, Chem. Phys. Lipids 158 (2009) 54–60.

[19] L. Qiu, C. Buie, A. Reay, M. Vaughn, K. Cheng, Molecular dynamics simulations reveal the protective role of cholesterol in β-amyloid protein-induced membrane disruption in neuronal membrane mimics, J. Phys. Chem. B 115 (2011) 9795–9812.

[20] J.A. Lemkul, D.R. Bevan, Perturbation of membranes by the amyloid β-peptide—a molecular dynamics study, FEBS J. 276 (2009) 3060–3075.

[21] C. Poojari, A. Kukol, B. Strodel, How the amyloid-β peptide and mebranes affect each other: an extensive simulation study, Biochim. Biophys. Acta 1829 (2013) 327–339.

[22] Y. Xu, J. Shen, X. Luo, W. Zhu, K. Chen, J. Ma, H. Jiang, Conformational transition of amyloid β-peptide, Proc. Natl. Acad. Sci. U. S. A. 102 (2005) 5403–5407.

[23] T. Pobandt, V. Knecht, Free energy of lipid bilayer defects affected by Alzheimer's disease associated amyloid-β42 monomers, J. Phys. Chem. B 118 (2014) 3507–3516.

[24] H. Jang, F.T. Arce, S. Ramachandran, R. Capone, R. Azimova, B.L. Kagan, R. Nussinov, R. Lal, Truncated β-amyloid peptide channels provide an alternative mechanism for Alzheimer disease and Down syndrome, Proc. Natl. Acad. Sci. U. S. A. 107 (2010) 6538–6543.

[25] T. Mori, J. Jung, Y. Sugita, Surface-tension replica-exchange molecular dynamics method for enhanced sampling of biological membrane systems, J. Chem. Theory Comput. 9 (2013) 5629–5640.

[26] C. Lockhart, D.K. Klimov, Alzheimer's Aβ10-40 peptide binds and penetrates DMPC bilayer: an isobaric-isothermal replica exchange molecular dynamics study, J. Phys. Chem. B 118 (2014) 2638–2648.

[27] J.F. Nagle, S. Tristram-Nagle, Structure of lipid bilayers, Biochim. Biophys. Acta 1469 (2000) 159–195.

[28] M. Buck, S. Bouguet-Bonnet, R.W. Pastor, A.D. MacKerell, Importance of the CMAP correction to the CHARMM22 protein force field: dynamics of Hen lysozyme, Biophys. J. 90 (2006) L36–L38.

[29] J. Klauda, R. Venable, J. Freites, J. O'Connor, D. Tobias, C. Mondragon-Ramirez, I. Vorobyov, J.A.D. MacKerell, R. Pastor, Update of the CHARMM all-atom additive force field for lipids: validation on six lipid types, J. Phys. Chem. B 114 (2010) 7830–7843.

[30] C. Lockhart, S. Kim, D.K. Klimov, Explicit solvent molecular dynamics simulations of Aβ peptide interacting with ibuprofen ligands, J. Phys. Chem. B 116 (2012) 12922–12932.

[31] C. Lockhart, D. Klimov, Molecular interactions of Alzheimer's biomarker FDDNP with Aβ peptide, Biophys. J. 103 (2012) 2341–2351.

[32] L. Kale, R. Skeel, M. Bhandarkar, R. Brunner, A. Gursoy, N. Krawetz, J. Phillips, A. Shinozaki, K. Varadarajan, K. Schulten, NAMD2: greater scalability for parallel molecular dynamics, J. Comp. Phys. 151 (1999) 283–312.

[33] Y. Sugita, Y. Okamoto, Replica-exchange molecular dynamics method for protein folding, Chem. Phys. Lett. 114 (1999) 141–151.

[34] H. Nymeyer, S. Ghanakaran, A.E. Garcia, Atomic simulations of protein folding using the replica exchange algorithm, Methods Enzymol. 383 (2004) 119–149.

[35] T. Okabe, M. Kawata, Y. Okamoto, M. Mikami, Replica exchange Monte-Carlo method for the isobaric–isothermal ensemble, Chem. Phys. Lett. 335 (2001) 435–439.

[36] C.B. Barber, D.P. Dobkin, H.T. Huhdanpaa, The Quickhull algorithm for convex hulls, ACM Trans. Math. Softw. 22 (1996) 469–483.

[37] P.A. Prakash, R. Sankararamakrishnan, Force field dependence of phospholipid headgroup and acyl chain properties: comparative molecular dynamics simulations of DMPC bilayers, J. Comp. Chem. 31 (2010) 266–277.

[38] C.R. Sanders, Solid state ^{13}C NMR of unlabeled phosphatidylcholine bilayers: Spectral assignments and measurements of carbon–phosphorus dipolar couplings and ^{13}C chemical shift anisotropies, Biophys. J. 64 (1993) 171–181.

[39] A. Ferrenberg, R. Swendsen, Optimized Monte Carlo data analysis, Phys. Rev. Lett. 63 (1989) 1195–1198.

[40] J. Chang, S. Sandler, Determination of liquid–solid transition using histogram reweighting method and expanded ensemble simulations, J. Chem. Phys. 118 (2003) 8390–8395.

[41] P. Conrad, J. de Pablo, Comparison of histogram reweighting techniques for a flexible water model, Fluid Phase Equilib. 150–151 (1998) 51–61.

[42] J.-P. Douliez, A. Leonard, E.J. Dufourc, Restatement of order parameters in biomemranes: calculation of C–C bond order parameters from C–D quadrupolar splittings, Biophys. J. 68 (1995) 1727–1739.

[43] D.P. Tieleman, L.R. Forrest, M.S.P. Sansom, H.J.C. Berendsen, Lipid properties and the orientation of aromatic residues in OmpF, Influenza M2, and alamethicin systems: molecular dynamics simulations, Biochemistry 37 (1998) 17554–17561.